DYNAMIC STALL EFFECTS AND APPLICATIONS TO HIGH PERFORMANCE AIRCRAFT

by
Jay M. Brandon
NASA Langley Research Center
Mail Stop 355
Hampton, Virginia 23665

SUMMARY

This paper highlights recent research conducted at the NASA Langley Research Center on the effects of large-amplitude pitching motions on the aerodynamic characteristics of modern fighter airplane configurations. Wind tunnel tests were conducted on simple flat-plate wings to gain understanding of the complex flow phenomena during unsteady motions at high angles of attack. Studies then progressed to a representative modern fighter configuration. Using a computer controlled dynamic apparatus, tests were conducted to investigate effects of pitch rate and motion time history, and to determine the persistence of unsteady effects. Data were also obtained in sideslip and with control surface deflections to investigate dynamic effects on lateral stability and available control power. Force and moment data were obtained using a 6-component internal strain-gage balance. To aid in the interpretation of the results, flow visualization using a laser light-sheet system was also obtained. Results of these tests will be discussed, along with their implications on the maneuverability of future advanced airplanes designed to operate in the highly dynamic, high angle-of-attack environment.

SYMBOLS

c	mean aerodynamic chord, ft
C_D	drag coefficient
C_l	rolling moment coefficient
C_L	lift coefficient
C_M	pitching moment coefficient
C_N	normal force coefficient
k	reduced frequency, $\frac{\omega c}{2V}$
L/D	lift-to-drag ratio, C_L/C_D
q	pitch rate, rad/sec
$\hat{q}$	non-dimensional pitch rate, $\frac{qc}{2V}$
t	time, sec
t_c	convective time unit
V	free stream velocity, ft/sec
α	angle of attack, deg
α_0	mean angle of attack
ω	oscillation frequency, rad/sec
LEX	leading-edge extension

INTRODUCTION

At high angles of attack, unsteady aerodynamic effects may have a major impact on the maneuverability and controllability of an airplane. Currently, some modern fighter airplanes are capable of performing transient maneuvers involving high pitch rates to extreme angles of attack; this has been graphically demonstrated in the so-called "Cobra maneuver" flown by Soviet aircraft at recent airshows. The advent of innovative high-α control effectors such as thrust vectoring and forebody controls will enable ever greater capability to effectively exploit a substantially enlarged envelope for air combat. With the emphasis on aggressive maneuvering capability near or beyond the stall angle of attack for future airplanes, research is needed to understand the effects of large-amplitude unsteady motions at high angles of attack on stability, control and performance.

A recent paper (ref 1) discussed the potential tactical benefits of unsteady aerodynamic phenomena; however, little research has been conducted on realistic three-dimensional configurations to quantify unsteady effects or to develop an understanding of the flow mechanisms involved. Additionally, the impact of unsteady aerodynamic effects on airplane flight dynamics (including stability and control effects during rapid high angle-of-attack maneuvers), and a practical means of utilizing these unsteady effects have to be addressed (ref 2).

A significant amount of research has been conducted in the area of unsteady aerodynamics at high angles of attack. However, most of the work to date has been on two-dimensional airfoils. These results show substantial force overshoots for pitching and plunging airfoils (refs 3-5). Current design trends for advanced airplane configurations show a clear need for extending the research to three-dimensional airplane configurations. Wind tunnel experiments have been conducted using delta wings undergoing pitching and plunging oscillations to determine vortical flow characteristics during large-amplitude motions (refs 6-8). The primary focus of the studies was the dynamics of the leading-edge vortex while the wing was undergoing motion. Under these conditions, the vortex burst point location was observed to lag the static location during pitch-up and pitch-down motions. Water tunnel results (ref 9) have shown vortex lag times of up to 30 convective time units (time required for an air particle to travel across the wing), which is a much slower response than that normally associated with two-dimensional dynamic stall phenomena. More recently, research was conducted on a series of wings of different sweep angles which showed that the magnitude of the unsteady aerodynamic effects decreased as the sweep angle increased (ref 10). Additional tests of semi-span models with various wing sweeps were reported in reference 11. Reference 12 extended this work to a representative three-dimensional configuration, tested at zero sideslip and with no control deflections, which showed significant force and moment increments due to dynamic stall effects. Measured persistence times of the dynamic effects were also presented. Reference 13 presented detailed wing surface pressure measurements of a straked-wing fighter model undergoing pitch oscillations. Force and moment measurements from water tunnel studies with a series of straked-wing models have been reported in reference 14.

This paper presents a summary of low-speed wind-tunnel tests of flat-plate wings and of a modern fighter configuration undergoing large-amplitude pitching

motions over an angle-of-attack range from 0° to 75°. Fundamental flow characteristics associated with dynamic stall are most evident in the simple wing models; however, those phenomena are also observed in the more complex actual aircraft geometry. This research has provided fundamental information on dynamic stall aerodynamics and potential impact on maneuvering flight dynamics of modern fighter aircraft. Much additional work is needed to enable accurate prediction of these effects, to provide reliable design methods, and to develop flow control concepts to exploit these dynamic phenomena for maneuvering enhancement.

FLAT-PLATE WING PLANFORMS

Low-speed wind tunnel tests were conducted on three flat-plate wing planforms to study basic 3-D dynamic stall flow mechanisms, and the effect of wing sweep on these phenomena. The three models, with wing sweeps of 70°, 45° and 0°, were tested on a pitch oscillation rig which oscillated the model sinusoidally at various reduced frequencies and about various mean angles of attack. A photograph of the models is shown in figure 1. The amplitude of the oscillations was held constant for these tests at 18°. The mounting system oscillated the models about their 40%c location. The tests were conducted in the Langley 12-Foot Low-Speed Wind Tunnel at a dynamic pressure of 4 psf resulting in a Reynolds number of 0.4×10^6 per foot.

Data recorded during test runs included a potentiometer reading of the oscillation rig pitch angle, 6-component force and moment data from the strain-gage balance, and tunnel dynamic pressure. These inputs were obtained at a rate of 100 samples/sec per channel. All input signals were electronically filtered by a 10 Hz low-pass filter. After data acquisition, weight and inertia tares were subtracted and the data were reduced to coefficient form.

70° Delta Wing

It is well known that vortical flow plays a dominant role in the high angle-of-attack characteristics of modern fighter aircraft. Since the flow field over a 70° delta wing is dominated by the presence of a strong leading-edge vortex system, the flat plate wing is an effective tool for the study of unsteady effects on vortical flows.

Longitudinal Characteristics- As angle of attack was increased from 0°, the leading-edge vortex system began to develop on the wing. As angle of attack was further increased, the vortex burst point traveled forward onto the wing. Figure 2 shows the effect of angle of attack and pitch rate on vortex burst location as determined by flow visualization tests. Statically, at α=22.5°, the burst point of the leading-edge vortices reached the trailing edge of the wing. As angle of attack was further increased, the loss in vortex lift over the rear of the wing due to the burst vortices resulted in a decrease in the CL-α slope and an increase in the nose-up pitching moment. At α=42°, the static vortex burst point reached the apex of the wing, and the flow field over the wing was characterized by fully separated flow.

Numerous studies have documented the hysteresis and overshoot characteristics exhibited by delta wings undergoing oscillations. Figure 2 shows the flow mechanism responsible for observed dynamic effects. The effect of pitch rate can be seen by comparing the dynamic vortex burst point positions with the static location. At a reduced frequency of k=.0426, during pitch-up motion, the dynamic burst point position lagged the static location by approximately 24% chord at 32° angle of attack. As reduced frequency was increased, the lag in the burst point location increased. As the model motion reversed direction and started to pitch down, the vortex burst point again lagged the static value for the remainder of the pitch oscillation cycle. At the faster reduced frequency, it was seen that the vortex burst point never reached the apex of the wing.

The vortex flow lags, and their resultant impact on aerodynamic forces and moments have been observed to be dependent on a number of factors including pitch rate, angle-of-attack range, and motion time history. Figure 3 shows a comparison of normal force coefficient for oscillations about various mean angles of attack from 22° to 37°. These data show that as the model was oscillated at high angles of attack, the overshoot and hysteresis loop was enlarged. The increase in overshoot due to the increase in mean angle of attack is due, in part, to the increase of pitch rate which occurred closer to the maximum static C_N as the mean angle of attack was increased. The hysteresis loop widened as the angle-of-attack range extended to higher values, due to more complete flow separation on the upper surface of the wing and the lags associated with the separation and reattachment process. As oscillation frequency was increased, the hysteresis loops and overshoot also increased due to the increased lag in vortex breakdown and redevelopment. A summary of the normal force overshoot for a range of reduced frequencies is shown in figure 4.

Lateral Characteristics- The vortex flow over the model also dominated the lateral stability characteristics. Figure 5 shows the burst locations of the vortices on the leeward and windward sides of the model under static conditions. As angle of attack was increased over 20°, the windward vortex burst point progressed forward onto the wing surface resulting in a loss of vortex lift on the windward side of the wing. This asymmetric loss of lift resulted in destabilizing increments to C_l as angle of attack increased. At α=30°, the leeward vortex burst point moved onto the wing and began a progression towards the apex as angle of attack was further increased. Again, this resulted in an asymmetric loss of vortex lift which gave a stabilizing increment to C_l. Above α=40°, very little vortex lift remained on either the windward or leeward sides of the wing and C_l assumed an essentially constant value. Dynamic lateral stability characteristics obtained by oscillating the model at β=5° are shown in figure 6. The effect of the oscillatory motion on roll stability was to delay the static characteristics which, as previously seen, were largely determined by the vortex burst point locations. Figure 6 shows the effect of frequency on lateral stability at a mean angle of attack of 27° and at 5° sideslip. The data show a delay in the reduction of stability compared to the static data at the mid angle-of-attack range; however, the dynamic data was much

less stable than the static data at the higher angles of attack. During the pitch-down phase, the dynamic data showed little effect of the asymmetric vortex breakdown progression as was discussed for the static and pitch-up data. The absence of variation of rolling moment during the pitch-down cycle was due to the delay in vortex formation on the upper surface of the wing. During the pitch-down cycle, the vortex burst points were much nearer the wing apex than for the upstroke or static cases, resulting in reduced forces and moments from asymmetric flow conditions. As the positive pitch rate was increased, the lateral stability improved progressively over the mid angle-of-attack range and the unstable increment at high angles of attack decreased.

Flow visualization provided information on the extent of the lag of the vortex burst point locations in sideslip. A comparison between figures 7 and 2 shows the effects of pitch rate on the asymmetric burst point locations in sideslip. As would be expected, for both static and dynamic conditions, the windward vortex burst at a point forward of the leeward vortex burst point. During oscillatory motion, the lag in the vortex burst point was evident in both windward and leeward vortex systems.

Effect of wing sweep

Modern fighter aircraft geometries consist of highly swept strakes, forebodies, and leading-edge wing extensions which generate concentrated vortical flow fields similar to the previously discussed 70° delta wing. In addition to the vortical flow fields, these aircraft can also incorporate moderately swept wings and tail surfaces which create a hybrid flow system over the configuration. To further understand the dynamic effects on wings with lower sweep angles, tests were also conducted on flat-plate wings with 45° and 0° leading-edge sweep angles. A photograph comparing the three wings tested was shown in figure 1. The two delta wings had the same wing area, and the rectangular wing had an aspect ratio of 1.46 which corresponds to the aspect ratio for the 70° delta wing.

As sweep angle is reduced, the flow field over the wing becomes more 2-dimensional in nature. Previous airfoil studies have documented the dynamic stall process for 2-dimensional configurations. The longitudinal force results for the airfoils showed trends similar to those observed for the 70° delta wing including large hysteresis loops and overshoots; however the mechanism responsible is quite different. Figure 8 shows a comparison of the two dynamic stall mechanisms. For the 2-D airfoil, as the airfoil flow separated during pitch-up, a dynamic stall vortex forms near the leading edge. This vortex grows as angle of attack increases, and then separates from the leading edge and convects downstream. A trailing-edge vortex also develops momentarily at high angles of attack. It is this dynamic stall vortex system which is responsible for the force overshoots and hysteresis seen for airfoils. This mechanism is contrasted to that discussed previously for the 70° wing. The 2-D dynamic stall characteristics are dominated by the presence of vorticity developed by flow separating at the leading edge and convecting downstream over the surface of the airfoil. For the 70° delta wing, the primary mechanism responsible for the dynamic stall effects was lags in the burst point location of the established leading-edge vortex system on the wing. For 3-dimensional, rectangular wing configurations, reference 15 reported that the inboard section of the wing produced flow which was essentially 2-D in nature; however, near the wing tip the dynamic stall vortex interacted with the tip vortex which behaved similarly to the observed leading edge vortex system on the 70° delta wing. The presence of the two types of flowfields provides a further challenge to the understanding of the unsteady aerodynamic effects associated with dynamic stall.

Longitudinal Characteristics- A comparison of the static normal force results between the three wings is shown in figure 9. As sweep angle was decreased, the maximum normal force coefficient and stall angle of attack were reduced due to the well known vortex lift which occurs on swept wings at high angles of attack. Dynamic normal force characteristics for the 45° and 0° sweep configurations ares shown in figures 10 and 11. These data show similar qualitative results to those seen previously for the 70° delta wing. Figure 12 shows a comparison of the maximum overshoot in normal force due to dynamic effects for the three flat-plate wings. The rectangular wing exhibited the largest overshoot and hysteresis effects due to pitch oscillation. This overshoot was due to the delay in flow separation and reattachment on the upper surface of the wing and the dynamic stall vortex, similar to the flow discussed earlier for airfoil dynamic stall. Because of the lower sweep angle, the 45° delta wing developed a less concentrated leading-edge vortex system which broke down at substantially lower angles of attack compared to the 70° wing. Additionally, the 45° sweep angle prevented large 2-D type of dynamic vortex lift to develop resulting in a hybrid flow situation somewhere in between the leading-edge dominated flow field of the 70° wing, and the quasi 2-D flow of the rectangular wing. The results clearly show that the dynamic stall effects decrease with increasing wing leading-edge sweep.

Lateral Characteristics- The effect of wing sweep on lateral stability is illustrated by comparing figures 5, 13, and 14. As noted previously, the asymmetric burst of the leading-edge vortices is the primary factor in the static lateral stability of wings with substantial sweep angle. Figure 13 shows that the 45° swept wing was fairly insensitive to dynamic effects on lateral stability. Because the moderate sweep angle does not develop the concentrated leading-edge vortex system, the asymmetric vortex structure over the wing and the lag in the vortex burst point locations during pitching oscillations, which were seen to cause the large changes in lateral stability for the 70° wing configuration, did not develop to a significant degree on the 45° wing. Figure 15 shows a sketch of the rectangular wing flow field in sideslip. The windward edge of the rectangular wing became a highly swept surface in sideslip, generating a vortex which passed over the wing. Figure 14 compares the static and dynamic results of the rectangular wing at 5° sideslip. The dynamic data exhibits a very large amount of scatter denoted by the shaded area. The inconsistency of the data for this wing is interesting because the data indicate large deviations from static values during the oscillations. The data trend suggests that under dynamic conditions the windward side of the wing tends to stay attached to higher angles of attack thus providing increases in stability. As discussed previously, a vortex is probably present on the windward side due to the effective 85° sweep angle of

the windward tip. These results indicate the sensitivity of the unsteady aerodynamic effects to planform shape. Realistic airplane configurations will likely exhibit several of these basic types of vortical flow fields which can interact to produce highly complex dynamic stall phenomena.

REALISTIC AIRCRAFT CONFIGURATION

Low-speed wind tunnel studies were conducted to explore the effects of large-amplitude pitching motions on the aerodynamic characteristics of a modern fighter airplane configuration. A sketch of the F-18 configuration tested is shown in figure 16. The test configuration incorporated a moderately swept wing with a highly swept leading-edge extension (LEX). All data presented herein will be with the leading-edge flaps deflected to 34° and trailing-edge flaps set to 0°. Tests were conducted at 0° and 10° sideslip, and with deflections of ailerons and horizontal tails. The model was mounted on the dynamic test rig through a six-component strain-gage balance. The dynamic test rig was a computer controlled, hydraulically-actuated system which was sting-mounted on a C-strut support system in the NASA Langley 12-Foot Low-Speed Wind Tunnel. A sketch of the installation is shown in figure 17. The mounting arrangement rotated the model about the reference center of gravity location of 24%c and provided an angle-of-attack range from 5° to 75°. The combination of model pitch rates and tunnel speeds allowed for a realistic representation of full-scale maneuvering conditions within the capabilities of current and projected future high performance airplanes. Figure 18 compares non-dimensional pitch rate to equivalent full-scale pitch rate for a representative fighter airplane.

Force tests were conducted at a dynamic pressure of 4 psf resulting in a Reynolds number of 0.4×10^6 per foot. Static data were obtained over an angle-of-attack range of 5° to 75°. Dynamic data were obtained for both oscillatory and ramp motions; however, the current discussion will focus on constant pitch-rate ramp motions. Tests were conducted using a range of initial and final angles of attack and pitch rates. Dynamic data were measured at non-dimensional pitch rates varying from $\hat{q}$=0.0087 to 0.0260. Gravity and inertia tare values were determined by measuring the forces and moments during wind-off test runs. These data were subtracted from the wind-on dynamic data. Because of the relatively low test frequencies and small model weight, inertia tare corrections were small.

Data recorded during test runs included a linear variable differential transformer reading from the pitch rig to determine the pitch angle, 6-component force and moment data from the strain-gage balance, and tunnel dynamic pressure. These inputs were obtained at rates between 100 and 200 samples/second per channel, depending on the test condition. All channels were electronically filtered by a 100 Hz low-pass filter. Further digital filtering was applied during post-test data analysis. All moment data were referenced to the 24%c location.

Longitudinal Characteristics

Static results- The flow field over the model at high angles of attack was dominated by a strong vortex system generated by the LEX. This vortex system contributed both to increased lift and reduced pitch stability. Development of the LEX vortex system started at very moderate angles of attack. At these conditions, the vortex system trailed over the wing and passed just outboard of the vertical tails. With increasing angle of attack, breakdown of the vortices progressed forward such that the burst point moved over the wing and LEX. In addition, a second vortex system developed on the forebody which interacted with the LEX vortices. A detailed discussion of the high-α vortical flow phenomena at static conditions for this configuration is contained in reference 16. Static longitudinal force and moment data measured in the current tests are presented in figures 19 and 20. Figure 19 shows a linear variation in lift with angle of attack up to about 20°. At this point, a reduction in lift-curve slope was caused by progression of the LEX vortex burst point onto the wing, however, lift continued to increase until a maximum value was reached at about α=35°. Figure 20 shows pitching moment characteristics. The results indicate near neutral stability for angles of attack up to 40°. This characteristic was due in large part to the lift produced on the LEX ahead of the moment reference center. Above α=48°, which corresponds to the condition at which the vortex burst point reached the LEX apex, the data show a substantial increase in pitch stability.

Dynamic results- A series of tests using constant pitch rate motions were conducted to investigate the effects of pitch rate and motion time history, and to determine the persistence of the unsteady aerodynamic effects. Pitch motions were generated starting from various angles of attack and at non-dimensional pitch rates from $\hat{q}$=0.0087 to $\hat{q}$=0.0260. Tests were conducted at both positive and negative pitch rates.

The effects of positive pitch rate on longitudinal characteristics are shown in figures 21-23. The model was pitched at constant pitch rates over an angle-of-attack range from 5° to 75°. Figure 21 shows an increase in lift coefficient due to pitch rate over the entire range of motion. A maximum increment of roughly 0.6 in C_L was observed for the highest pitch rate case as compared with static values, and the maximum increment occurred beyond the angle of attack for maximum lift. The figure shows that as pitch rate was increased, the increment in C_L increased. Although the lift enhancement would be expected to peak at some value of pitch rate, the range of rates tested did not determine the pitch rate beyond which no further increase in lift occurred. Figure 22 shows the effect of pitch rate on the drag polar of the model. These data show substantial decreases in drag for a constant lift coefficient at angles of attack below maximum lift. It is also noted that beyond maximum lift, in addition to the increased values of lift coefficient, dynamic effects produced correspondingly high values of drag. Figure 23 shows the effect of positive pitch rate on pitching moment. As discussed in reference 12, a number of factors must be considered when analyzing these data including the distribution of induced angle of attack generated over the model due to the pitch rate, and the flow lag associated first with flow separation and vortex formation at the lower angles of attack, and then with vortex breakdown at the higher angles of attack. The data presented in figure 23 show that for all angles of attack up to 50°, the ramp motions produced large nose-down C_M increments compared to the static values. At the lower

angles of attack, this effect was found to be largely due to the induced angle-of-attack distribution discussed earlier which tended to increase loads on the horizontal tails producing nose-down C_M increments. At the higher angles of attack, however, the lag in the breakdown of the LEX vortex system became dominant. The lag in the LEX generated flow field resulted in the nose-up pitching moment increments seen above about α=55°. Under static conditions, the LEX vortex burst point reached the apex of the LEX at about α=48°, reducing lift on the forward region of the model which resulted in a net pitch-down increment. During pitch-up motion, the established vortex flow remained intact to higher angles of attack and therefore the sharp pitching moment break exhibited statically above α=48° was substantially delayed.

The effects of negative pitch rate on longitudinal characteristics while the model was pitched from 75° to 5° angle of attack are shown in figures 24-26. At α=75°, the flow condition on the model was characterized by complete flow separation and breakdown. During the pitch-down motion, the formation of the LEX vortex system lags in comparison to the static case and the reattachment of the wing flow is delayed. This resulted in large increments in the forces and moments compared to static values. Figure 24 shows the effect of negative pitch rate on lift coefficient. Large decreases in lift coefficient were evident due to the motion. As pitch rate was increased, the loss in lift increased due to the lags in vortex development and wing flow reattachment. Figure 25 shows the effect of negative pitch rate on the drag polar of the model. The flow characteristics discussed above resulted in little increase in lift during the pitch-down motion, and in very low L/D values compared to static data. Similar trends were seen in pitching moment characteristics during pitch-down motions. Figure 26 shows that the delay in the vortex formation on the LEX (forward of the moment reference center) resulted in a negative increment in C_M from 60° to 40° angle of attack. Further in the pitch-down cycle, the LEX vortex system developed; however, the burst location was much further forward than for the static condition. The forward location of the LEX vortex system resulted in the positive increment in C_M seen from 40° to 0° angle of attack.

A comparison of effective pitch damping characteristics was made between current results and data from conventional small-amplitude forced oscillation tests. Figure 27 summarizes these results. In order to directly compare results from the two different test techniques, a pitch damping derivative was calculated from the current data by subtracting static values from the dynamic results. This difference was then non-dimensionalized to obtain a pitch damping derivative. A comparison was made between the two test techniques for both pitch-up and pitch-down motions. Because of the assumed linearity of pitch damping with pitch rate, inherent in the conventional forced oscillation results, the predicted pitch damping derivative from this test is identical for both positive and negative pitch rate motions. The comparison shows that during pitch-up motions, large amplitude and conventional results agreed closely below α=50°. Above α=50°, the large amplitude results indicate slightly less damping than predicted by conventional tests. During pitch-down motions, the current results show large differences in damping compared to the forced oscillation results. This difference reflects the importance of motion time history on dynamic stall phenomena.

To aid in the interpretation of the force and moment results, flow visualization was conducted using a pulsed laser light sheet system. Figure 28 shows a comparison of static and pitching motions at 30° angle of attack at a station corresponding to the junction of the wing leading edge and the fuselage. The pictures show that compared to the static case, the upward motion developed a vortex core which was slightly closer to the model surface (fig 28 b), and the burst point of the LEX vortex was seen to be substantially more aft. Conversely for the pitch-down case, the vortex core has burst at this location (fig 28 c).

In addition to the lag and overshoot characteristics, two other important attributes of dynamic stall need to be considered. The first is the previously mentioned impact of motion time history on the dynamic effects. Because dynamic stall phenomena are essentially flow lag effects, the past time history of the motion can play an important role in determining the characteristics. As an example, figure 29 shows normal force coefficient for a series of three constant pitch rate motions starting at different angles of attack. At a given angle of attack, all three dynamic motions had identical values of pitch rate; however, as can be seen, substantial differences in forces existed between the motions. This is due to the differences in the initial flow field condition over the model before the motion began. These types of effects are not currently captured in the aerodynamic mathematical models used in aircraft simulations. The second important attribute of dynamic stall effects is the persistence of the effects. The identification of persistence times is an essential ingredient in predicting the importance of dynamic stall effects on airplane capabilities. Obviously, in order to have an impact on the flight dynamics of the airplane, the force and moment increments induced by dynamic stall effects must persist long enough to integrate into displacement of velocity or rotational vectors. Persistence is usually measured in convective time units. One convective time unit is defined to be equal to the amount of time it takes for an air particle to travel across the mean aerodynamic chord of the wing. Figure 30 shows the relationship between convective time units and actual time for a full-scale F-18 airplane. Tests with the current configuration have shown persistence to be a function of pitch rate, angle-of-attack range, and motion time history. Figure 31 shows the persistence of the lift overshoot for two pitch rates and two final angles of attack. The data show that the maximum persistence times achieved were near 80 convective time units. The largest persistence values were obtained when the model motion was stopped at an angle of attack of 45°. This corresponds to the point at which the largest dynamic increment was seen (figure 21). Preliminary analysis (ref 12) which took into account only lift characteristics, has shown that persistence values obtained in these tests were too short to significantly enhance maneuver capability of this airplane.

Lateral Characteristics

In addition to longitudinal stability and performance aspects, the impact of dynamic stall effects on lateral

stability may also be important. It is well known that the forebody and LEX flow fields play a dominant role in the lateral stability characteristics of modern fighter configurations at high angles of attack; therefore, the vortex lag effects seen previously would be expected to influence lateral stability as well as longitudinal stability.

Static results- Figure 32 shows the static rolling moment coefficient for sideslip values of 0° and 10°. Focusing on the 10° sideslip case, the progression of LEX vortex burst over the wing can be seen. Typical of swept wing configurations, as angle of attack was increased from 5° to 15° an increase in lateral stability was seen. As angle of attack was further increased, the windward vortex system burst point reached the trailing edge of the wing and progressed forward, reducing lift on the windward side and thereby decreasing the rolling moment coefficient. Beyond 35° angle of attack, the leeward LEX vortex burst point moved forward onto the wing reducing lift on the leeward side which resulted in an increase in static roll stability.

Dynamic results- To assess the effects of pitch rate on the lateral stability characteristics, the model was pitched at constant rates over an angle-of-attack range from 5° to 75° and 75° to 5° at several values of sideslip. The data exhibited large differences in rolling moment due to pitch rate. The dynamic rolling moment characteristics reflected the effect of flow lags similar to what was discussed earlier for the 70° delta wing. Figure 33 shows the effect of positive pitch rate on lateral stability at 10° sideslip. As previously discussed, during pitch-up motions vortex bursting and wing flow separation is delayed to higher angles of attack compared to static conditions. At sideslip, this resulted in a delay of windward wing lift loss which, in turn increased stable dihedral effect (negative C_l), and also extended the conventional low angle-of-attack range where lateral stability increased with increasing angle of attack. As pitch rate was increased, the magnitude of the dynamic increments in rolling moment increased.

In addition to lags in the windward vortex, delay of the leeward vortex burst was also evident. This effect can most easily be seen in the data at the lowest pitch rate, $\hat{q}$=0.0087. The data show that over the angle-of-attack range from 30° to 50° the delay in the burst of the leeward vortex system resulted in a destabilizing rolling moment contribution.

At negative pitch rates (figure 34), the model motion was initiated at conditions of fully separated flow. As the model was pitched towards lower angles of attack, lag in the redevelopment of vortical flow over the model resulted in large variations in rolling moment compared to static results. The data show that over a moderate angle-of-attack range from 25° to 40°, the motion produced substantial increments in negative C_l. This result suggests a relatively long delay in the reformation of the leeward vortex system.

Control Characteristics

Adequate control effectiveness must be maintained to achieve effective maneuver performance in the high angle-of-attack flight regime. As an airplane is conducting large-amplitude, high rate maneuvers at high angles of attack, dynamic stall effects may impact control effectiveness. Accurate predictions of the high-α agility of an airplane require understanding of dynamic stall effects on control characteristics. Tests were conducted to obtain an indication of dynamic effects on control effectiveness in the pitch and roll axes.

Pitch control power- A comparison of total available pitch control power between static and dynamic conditions is shown in figure 35. The difference between data obtained with full nose-up control (δ_h=-24) and that obtained with δ_h=0 resulted in the ΔC_M values shown in the figure. Values of ΔC_M were computed for both static and dynamic test conditions. The results showed that a slight increase in horizontal tail effectiveness was generated due to positive pitch rate at angles of attack below 62°. Part of the observed effect was due to the improved flow field conditions at the aft end of the model caused by flow lags previously discussed. Additionally, the change in the horizontal tail deflection slightly altered the pitch damping characteristics, which are an integral part of the dynamic data set shown in the figure.

Roll control power- Figure 36 shows a comparison of the static and dynamic rolling moment for a right roll control input (δ_a=-25°). The static data show a large roll control moment at angles of attack below 20°. Above α=20°, the roll control power rapidly declined due to the stall of the wing and breakdown of the LEX vortices above the wing. The dynamic data again showed the impact of flow lags. During pitch-up motion, the breakdown of the LEX vortex system over the wing was delayed. This resulted in a wing flow field condition corresponding to a lower angle of attack. Because of the delay in the wing flow field breakdown, aileron effectiveness remained at the low-α control levels to 30° angle of attack before declining. As angle of attack was further increased, the dynamic roll control effectiveness decreased, due to the vortex and wing flow field breakdown; however, the lags in the breakdown compared to static conditions resulted in a higher level of available roll control over most of the angle-of-attack range. During pitch down, the model motion was initiated in a region of fully separated flow. The pitch-down motion delayed the reformation of the flow field over the wing which resulted in a delayed increase in roll control power as angle of attack was reduced compared to static data.

Impact On Maneuvering Capability

A preliminary assessment of the potential flight dynamics impact of the unsteady aerodynamic effects discussed above was made by considering two fundamental high-α maneuvers. These maneuvers are nose pointing and velocity vector turning and are illustrated in figure 37 (see reference 2 for additional discussion).

Nose Pointing Capability- A rapid large-amplitude pitch-up maneuver to point the nose of the airplane at an adversary can be very effective in close-in air-to-air combat. The primary desired airplane characteristics to effectively perform this type of maneuver are the ability to generate large pitch accelerations and rates, and adequate levels of stability at the resulting high angles of attack. In addition, excessive build-up of

drag is undesirable due to the increased energy loss during the maneuver. The large-amplitude ramp motions explored in this study are representative of a nose-pointing maneuver. As discussed earlier, the data measured for this type of motion show a large increase in lift due to unsteady effects, and at the higher angles of attack, a marked increase in drag compared to static values (see figures 22 and 25). Of even greater importance perhaps, is the unsteady pitching moment characteristics. The data suggests that the effective pitch rate damping due to unsteady dynamic effects can vary widely from that measured in conventional wind tunnel testing involving small-amplitude motions. This result implies that the dynamic effects could inhibit the ability to generate the high controllable pitch rates and accelerations desired for effective nose pointing, or adversely affect the stability of the configuration during air combat maneuvering. These effects may have to be included in simulation studies for accurate prediction of these types of motions.

Velocity Vector Turning- As shown in figure 37, the other class of maneuver assessed was velocity vector turning. The ability to perform rapid, low radius turns is very advantageous in close-in air-to-air combat. The primary aerodynamic factor in turning performance is the level of lift that can be generated. Because unsteady aerodynamic effects can produce large increments in lift over the static values, there has been much speculation about the benefits in maneuverability which may be achievable utilizing these effects. Assuming an increment in lift of 0.5, approximately the maximum measured due to unsteady effects, potential turn performance improvements can be assessed. Figure 38 shows the instantaneous turn rate achievable for a baseline configuration (no unsteady aerodynamic effects) and for a configuration with an assumed 0.5 increment in C_L due to unsteady aerodynamics for a 32000 lb airplane at 10000 feet altitude. The upper boundary represents corner speed as dictated by limit load factor. The data show a significant increase in instantaneous turn rate due to the unsteady aerodynamic effects, and a reduction in corner speed. These improvements, however, are meaningful only if the persistence of the dynamic lift is sufficient to allow the forces to integrate into significantly improved turning angles compared to the baseline performance capability. A preliminary assessment of the required persistence was made using a very simplified analysis. The experimental data indicated that the lift bleedoff following motion cessation is approximately exponential. Thus this behavior was modeled as an exponential function as discussed in reference 12.

Using this model and a simple point mass analysis method, the effect of persistence on the turn performance of the airplane was addressed. Figure 39 shows the increased turn angle capability due to dynamic effects for various persistence times. These results suggest that for the dynamic lift effects to become significant in terms of a turning advantage, the required persistence of the unsteady effects would probably need to be in excess of 100 convective time units (incremental turn angle > 4°). As discussed earlier, maximum values of only about 80 convective time units were seen during the experiments. Thus it appears that the natural persistence of the dynamic lift overshoots is too low to provide significant turn benefits.

CONCLUDING REMARKS

Design trends for future fighter aircraft indicate continued emphasis on maneuver capability in the stall/post-stall high angle-of-attack flow regime. Aggressive exploitation of the high angle-of-attack envelope will likely encounter large unsteady aerodynamic effects. These effects need to be identified and analyzed in order to ensure that adequate predictions of airplane flight dynamics can be obtained.

This paper has summarized recent research at NASA Langley Research Center on the effects of dynamic stall on airplane characteristics at high angles of attack. Results have shown that fundamental flow field mechanisms which occur on simple flat-plate models are similar to those found on a realistic configuration. Substantial increments in lift, drag, and pitching moment due to dynamic effects were measured for the rapid large-amplitude pitching motions. Pitch rate was the dominant influence, however motion time history was also important.

The primary consideration of this research is the impact of dynamic effects on airplane flight dynamics. Natural persistence of the dynamic lift effects were seen to be too short to significantly affect turn performance; however, longitudinal and lateral stability were significantly impacted by dynamic effects. This latter characteristic may result in transient performance differences not currently predicted by conventional test techniques. In addition to force generation and stability impacts, dynamic stall effects also were apparent in control effectiveness in both pitch and roll axes.

Additional research is needed to determine the impact of the dynamic stall effects on both stability and control power and to explore flow control methods for exploiting these phenomena. Only by understanding the complex flow phenomena at high angles of attack, and their effects on flight dynamics during high rate maneuvering, can new aircraft be confidently designed to maneuver effectively and aggressively exploit this expanded maneuvering envelope.

REFERENCES

1. Lang, J.D.; and Francis, M.S.: Unsteady Aerodynamics and Dynamic Aircraft Maneuverability. AGARD CP-386, May 1985.

2. Nguyen, L.T.: Flight Dynamics Research for Highly Agile Aircraft. SAE paper 892235, September 1989.

3. Lorber, P.F.; and Carta, F.O.: Airfoil Dynamic Stall at Constant Pitch Rate and High Reynolds Number. AIAA 87-1329, June 1987.

4. Galbraith, R.A.; Niven, A.J.; and Seto, L.Y.: On the Duration of Low Speed Dynamic Stall. ICAS-86-2.4.3.

5. Francis, M.S. et al: An Investigation of Airfoil Dynamic Stall Overshoot of Static Airfoil Characteristics. AIAA-85-1773 August 1985.

6. Wolffelt, K.W.: Investigation on the Movement of Vortex Burst Position With Dynamically Changing Angle of Attack for a Schematic Deltawing in a

Watertunnel With Correlation to Similar Studies in a Wind Tunnel. AGARD CP-413, October 1986.

7. Lambourne, N.C. et al: The Behavior of the Leading-Edge Vortices Over a Delta Wing Following a Sudden Change of Incidence. ARC-R/M-3645 1970.

8. Gad-el-Hak, M.; and Ho, C.: The Pitching Delta Wing. AIAA Journal Vol. 23, No. 11, November 1985.

9. Reynolds, G.A.; and Abtahi, A.A.: Instabilities in Leading-Edge Vortex Development. AIAA-87-2424, August 1987.

10. Brandon, J.M.; and Shah, G.H.: Effect of Large Amplitude Pitching Motions on the Unsteady Aerodynamic Characteristics of Flat-Plate Wings. AIAA-88-4331, August 1988.

11. David, M.: Water Tunnel Investigation of the Vortex Dynamics of Periodically Pitched Wings. MS Thesis, Air Force Inst. Technol., December 1988. (Available from DTIC as AD-A206 359).

12. Brandon, J.M.; and Shah, G.H.: Unsteady Aerodynamic Characteristics of a Fighter Model Undergoing Large-Amplitude Pitching Motions at High Angles of Attack. AIAA-90-0309, January, 1990.

13. Cunningham, A.M.; and den Boer, R.G.: Harmonic Analysis of Force and Pressure Data Results For An Oscillating Straked Wing at High Angles. AIAA-87-2494, August, 1987.

14. Cunningham, A.M.; and Bushlow, T.: Steady And Unsteady Force Testing Of Fighter Aircraft Models In A Water Tunnel. AIAA-90-2815, August, 1990.

15. Robinson, M.E.; and Wissler, J.B.: Pitch Rate and Reynolds Number Effects On A Pitching Rectangular Wing. AIAA-88-2577, June, 1988.

16. Erickson, G.E.: Water Tunnel Flow Visualization and Wind Tunnel Data Analysis of the F/A-18. NASA CR-165859, May 1982.

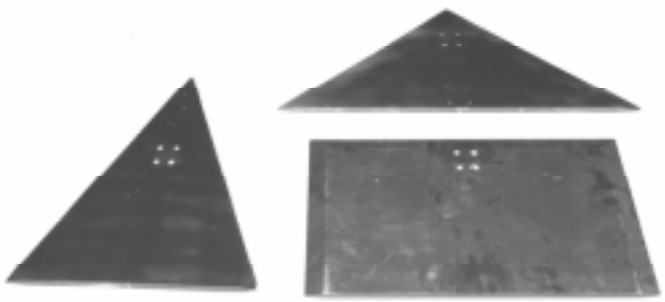

Figure 1 - Photograph of flat-plate models

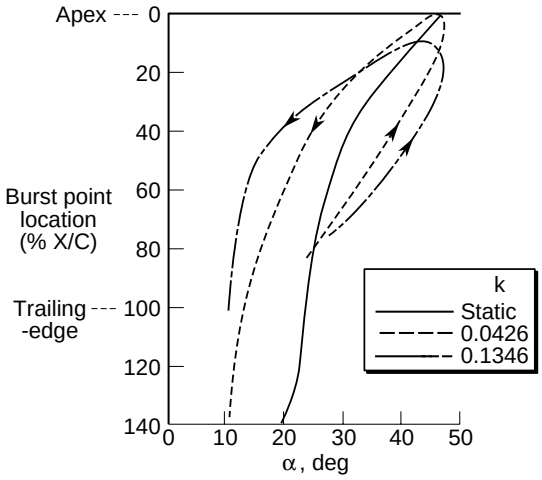

Figure 2 - Effect of pitch rate on burst point location, 70° delta wing

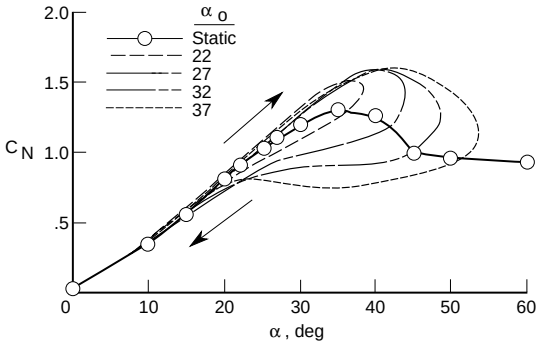

Figure 3 - Effect of mean angle of attack on dynamic force characteristics, 70° wing, k=0.0376

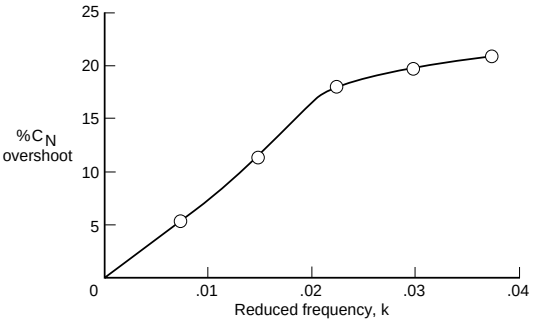

Figure 4 - Effect of pitch rate on normal force overshoot, 70° wing

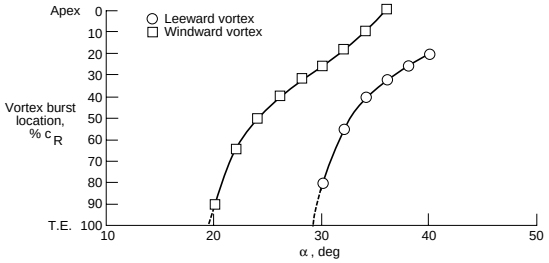

Figure 5 - Vortex burst location, 70° wing, β=5°

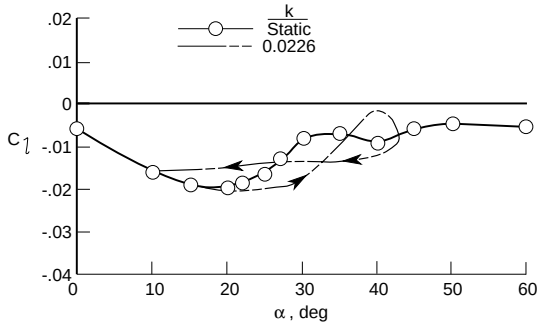

Figure 6 - Effect of pitch rate on lateral stability, 70° wing, α_0=27°, β=5°

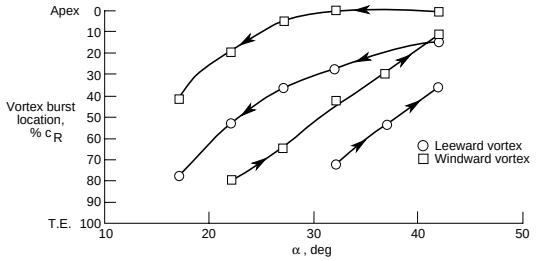

Figure 7 - Dynamic vortex burst location at sideslip, 70° wing, α_0=27°, β=5°, k=0.0426

<figure missing>

Figure 8 - Dynamic stall flow field mechanisms

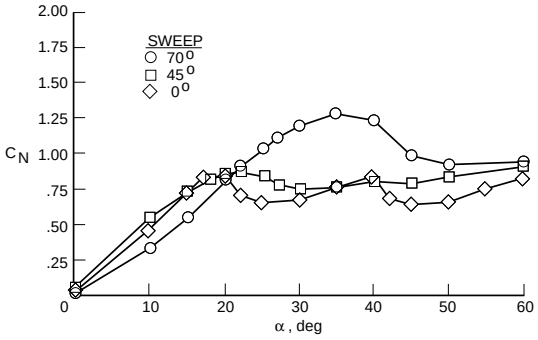

Figure 9 - Comparison of static normal force characteristics for flat-plate wings

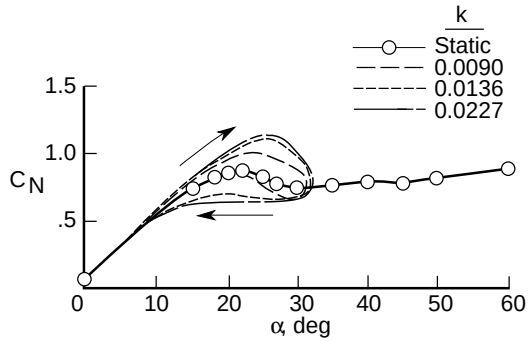

Figure 10 - Effect of reduced frequency on normal force coefficient, 45° wing

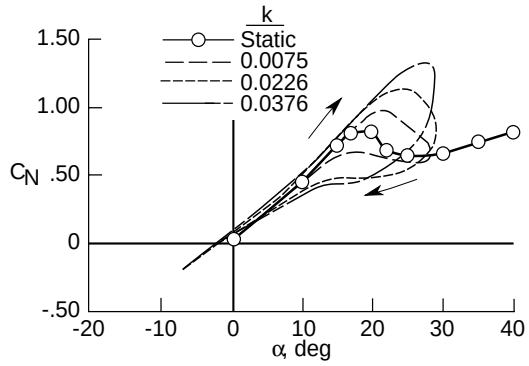

Figure 11 - Effect of reduced frequency on normal force coefficient, 0° wing

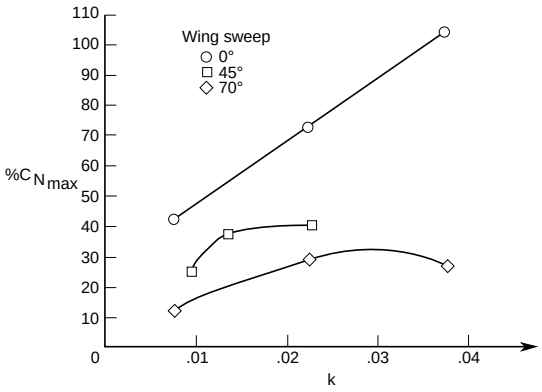

Figure 12 - Comparison of maximum normal force overshoot characteristics

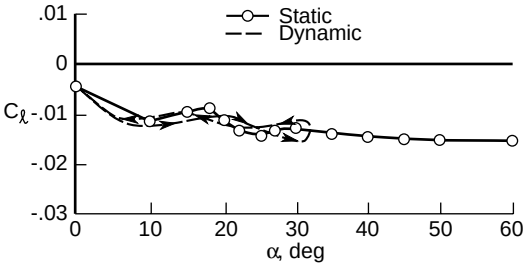

Figure 13 - Effect of pitch oscillation on lateral stability, 45° wing, α_0=15°, β=5°, k=0.0227

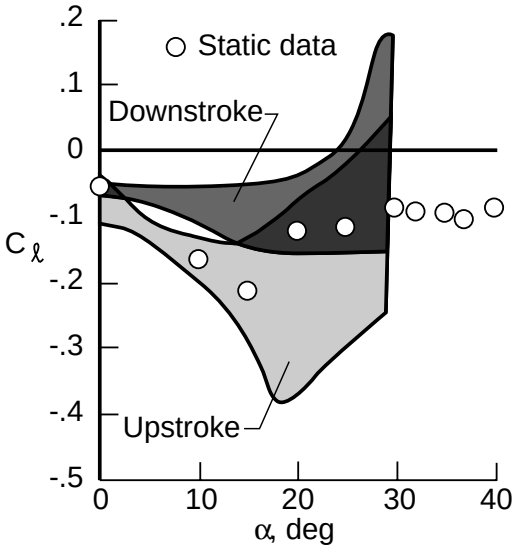

Figure 14 - Effect of pitch oscillation on lateral stability, 0° wing, α_0=12°, β=5°, k=0.0376

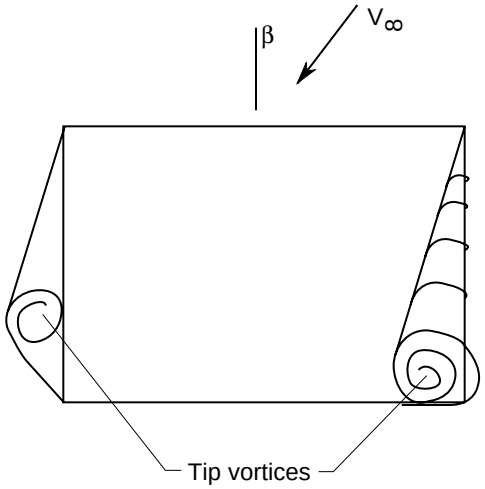

Figure 15 - Flow field in sideslip

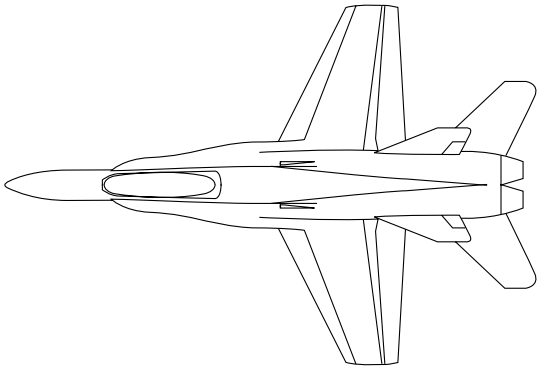

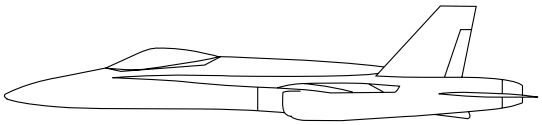

Figure 16 - Sketch of F-18 configuration

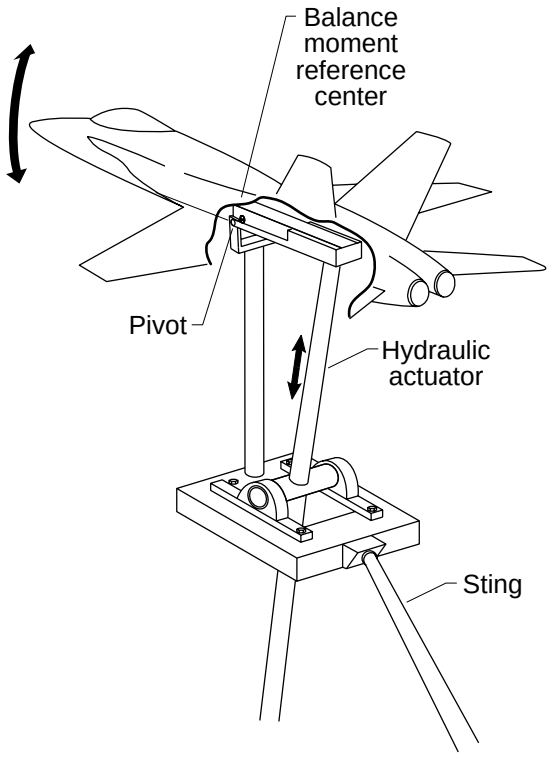

Figure 17 - Model installation

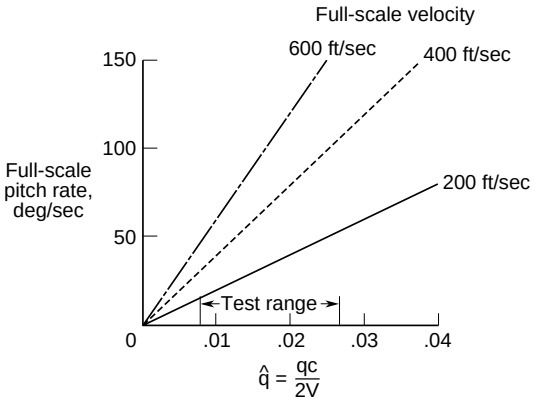

Figure 18 - Non-dimensional pitch rate

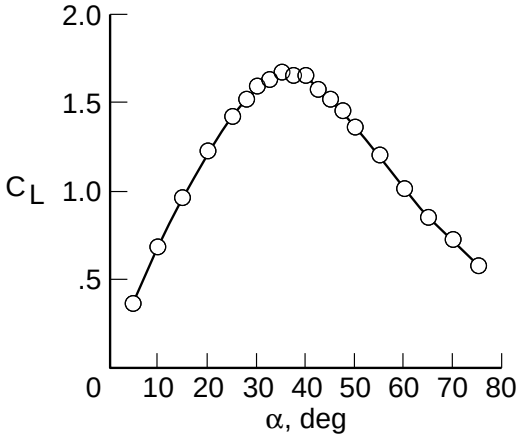

Figure 19 - Static lift characteristics, F-18 configuration

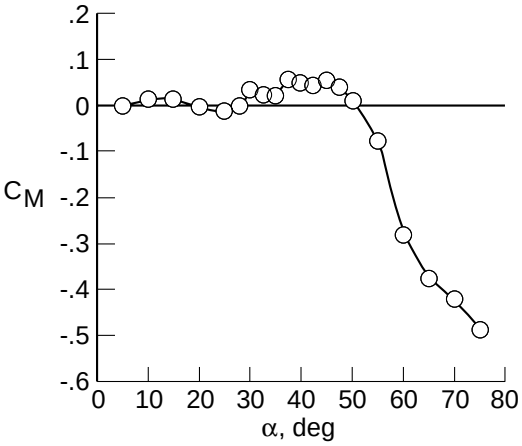

Figure 20 - Static pitching moment characteristics, F-18 configuration

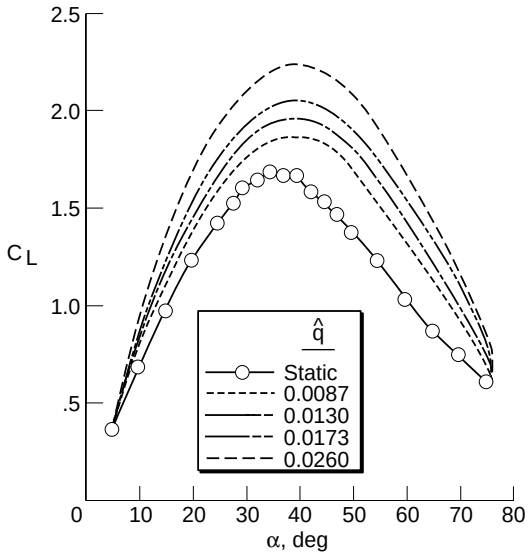

Figure 21 - Effect of positive pitch rate on lift coefficient

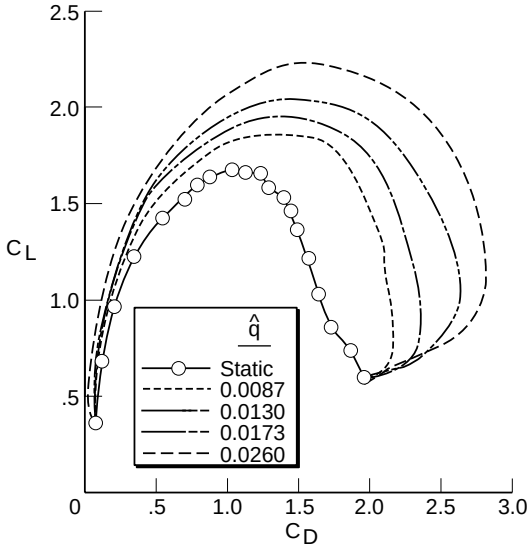

Figure 22 - Effect of positive pitch rate on drag polar

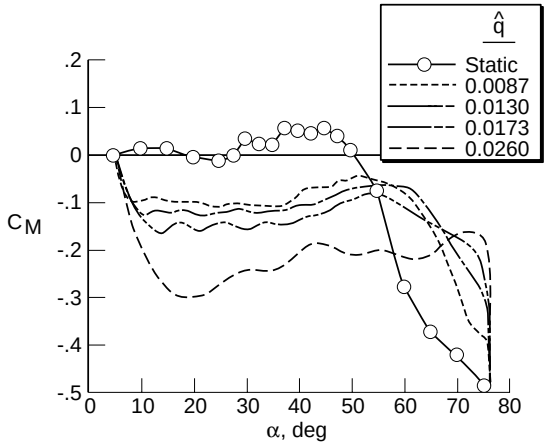

Figure 23 - Effect of positive pitch rate on pitching moment coefficient

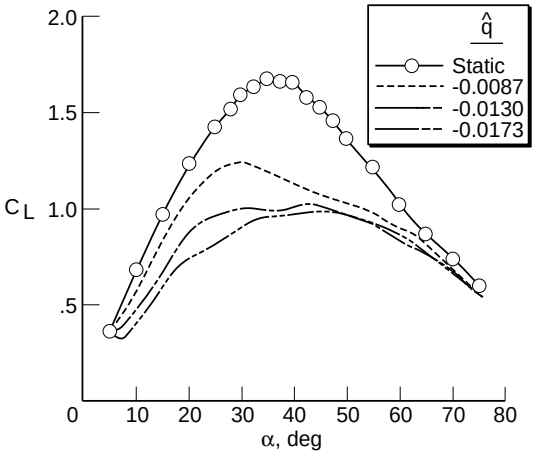

Figure 24 - Effect of negative pitch rate on lift coefficient

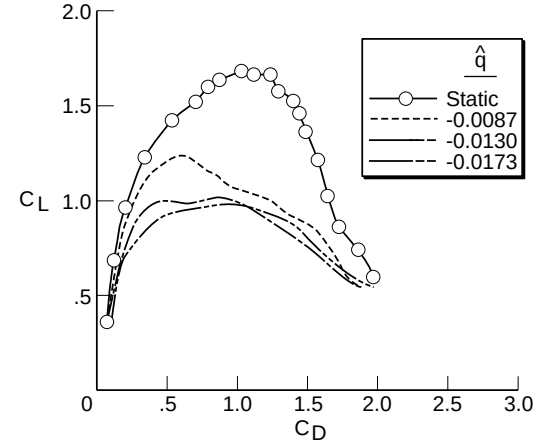

Figure 25 - Effect of negative pitch rate on drag polar

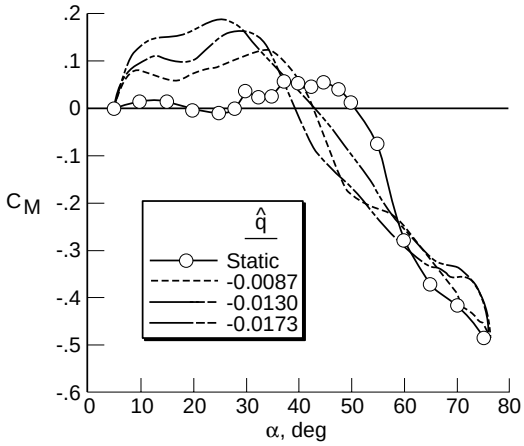

Figure 26 - Effect of negative pitch rate on pitching moment coefficient

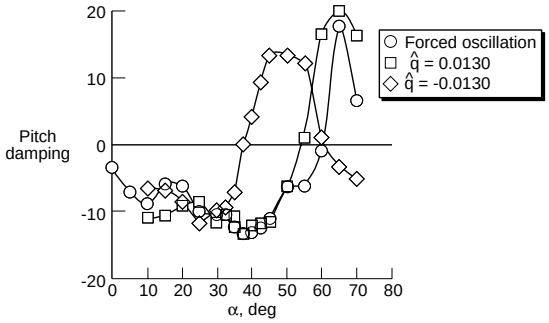

Figure 27 - Comparison of predicted pitch damping between conventional results and large-amplitude data

Figure 28 - LEX vortex flow visualization, α=20°
(a) Static

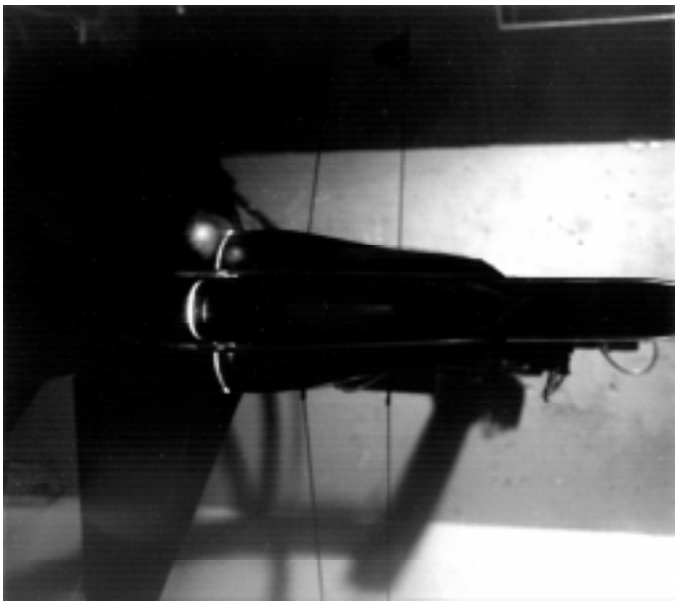

Figure 28 - Continued
(b) $\hat{q}$=0.0260

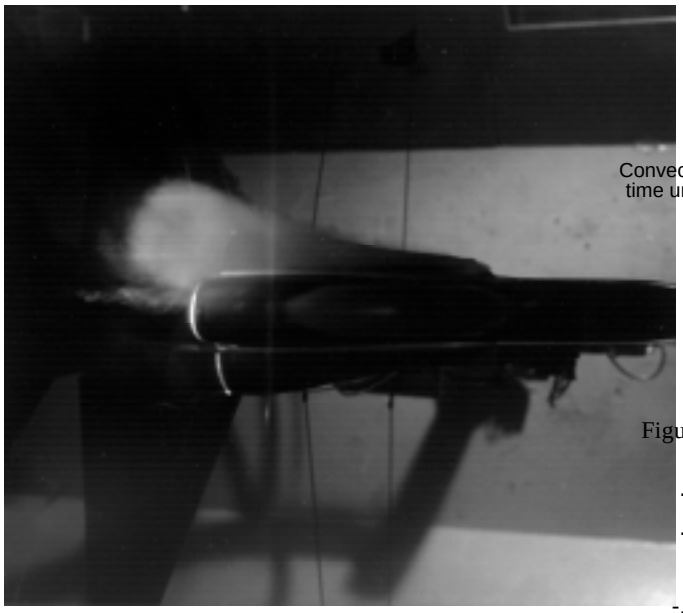

Figure 28 - Concluded
(c) $\hat{q}$=-0.0260

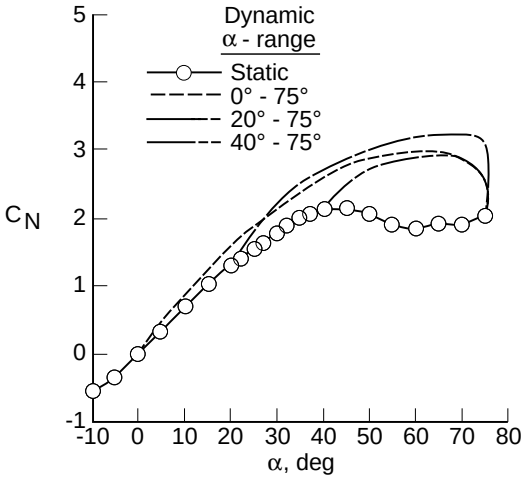

Figure 29 - Effect of motion time history

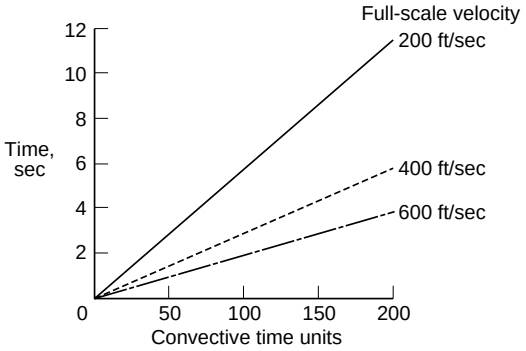

Figure 30 - Convective time relationship

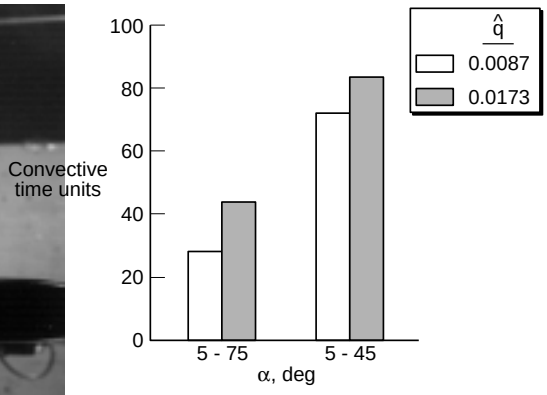

Figure 31 - Persistence for pitch-up motions

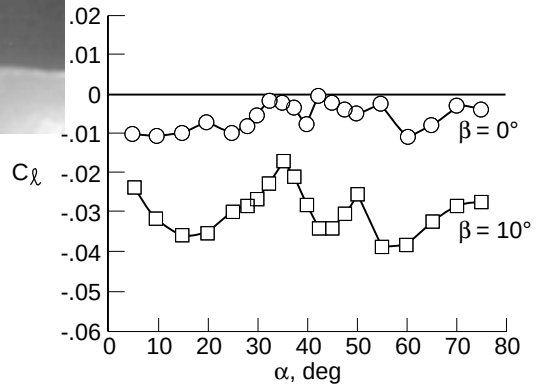

Figure 32 - Static rolling moment characteristics

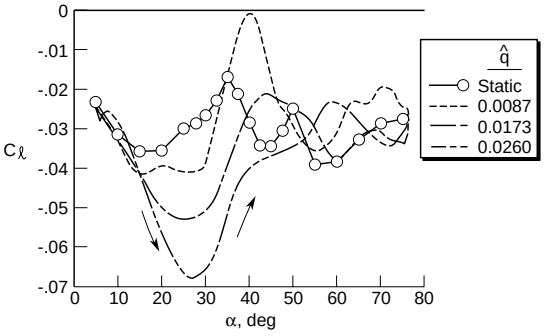

Figure 33 - Effect of positive pitch rate on lateral stability, β=10°

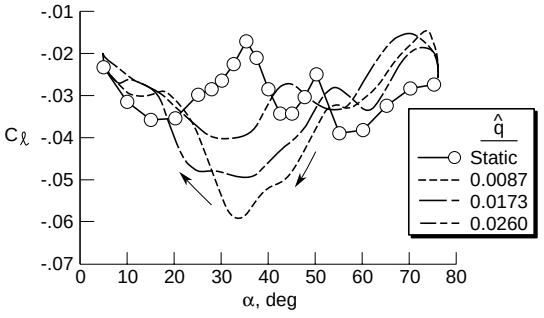

Figure 34 - Effect of negative pitch rate on lateral stability, β=10°

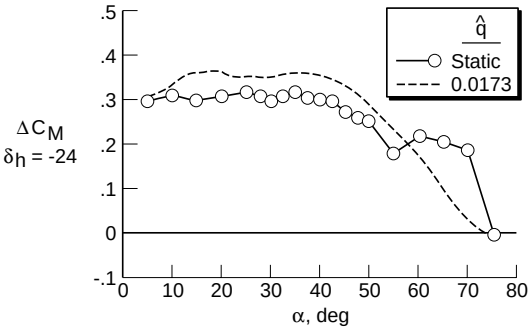

Figure 35 - Nose-up control power

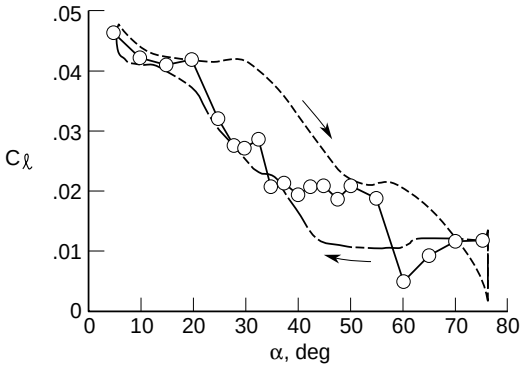

Figure 36 - Roll control characteristics, δ_a=-25°

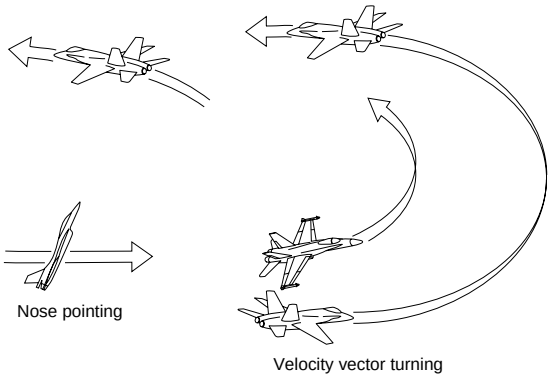

Figure 37 - Fundamental high-α maneuvers

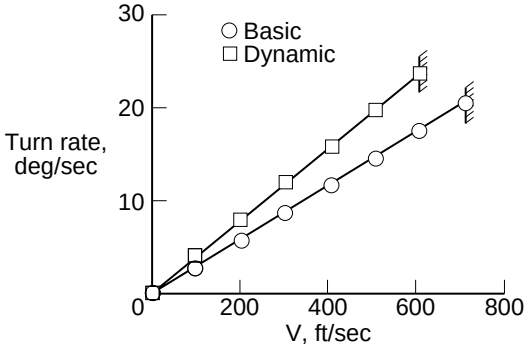

Figure 38 - Dynamic effects on instantaneous turn rate

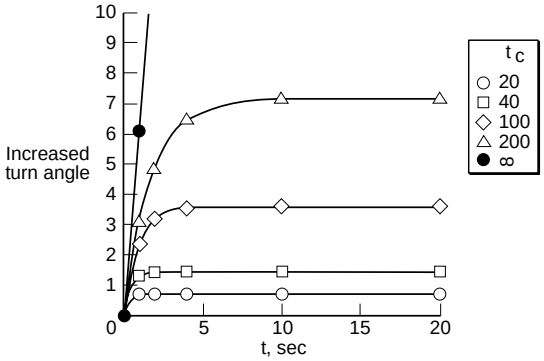

Figure 39 - Effect of dynamic lift persistence on turn performance